Final version published as: "Synthesis of Lithium Niobate Nanocrystals with Size Focusing through an Ostwald Ripening Process," Ali, R.F.; Gates, B.D., *Chemistry of Materials*, 2018, 30 (6), 2028-2035. https://doi.org/10.1021/acs.chemmater.7b05282

Synthesis of Lithium Niobate Nanocrystals with Size Focusing through an Ostwald Ripening Process

Rana Faryad Ali[†], *Byron D. Gates*[*,†]

[†] Rana Faryad Ali, Prof. Byron D. Gates
Department of Chemistry and 4D LABS
Simon Fraser University, 8888 University Drive
Burnaby, BC, V5A 1S6, Canada

[*] E-mail: bgates@sfu.ca

Abstract

A simple surfactant assisted solution-phase approach is demonstrated here for the preparation of lithium niobate ($LiNbO_3$) nanoparticles with an average size of 30 nm. This solution-phase process results in the formation of crystalline, uniform nanoparticles of $LiNbO_3$ at 220 ^oC with an optimal reaction time of 36 h. Advantages of this method also include the preparation of crystalline nanoparticles of $LiNbO_3$ without the need for further heat treatment or the use of an inert atmosphere. The growth of these nanoparticles began with a controlled agglomeration of nuclei. The reaction subsequently underwent a process of oriented attachment and Ostwald ripening, which dominated and controlled the further growth of the nanoparticles. These processes produced single-crystalline nanoparticles of $LiNbO_3$. The average dimensions of the nanoparticles were tuned from 30 to 95 nm by increasing the reaction time of the solvothermal process. The $LiNbO_3$ nanoparticles were characterized using transmission electron microscopy (TEM), selected area electron diffraction (SAED), high resolution TEM, X-ray diffraction, and Raman spectroscopy techniques. The nanoparticles were also confirmed to be optically active for second harmonic generation (SHG). These particles could enable further development of SHG based microscopy techniques.

Introduction

Single crystal lithium niobate ($LiNbO_3$) nanoparticles were prepared using a surfactant assisted solution-phase method. Lithium niobate based nanomaterials have attracted attention due to their wide range of applications in the fields of ferroelectrics,[1,2] piezoelectrics,[3] and non-linear optics.[4] Lithium niobate is a unique optical material. This material has been referred to as the 'silicon of photonics' due to its excellent optical properties.[5,6] Single crystals of $LiNbO_3$ are one of the most versatile and sought after non-linear optical (NLO) materials due to its large second order susceptibilities (e.g., 41.7 pm/V), photostability, and wide transmission window (e.g., 400 to 5000 nm).[7,8] Due to its NLO response, $LiNbO_3$ based materials are important components of wavelength conversion devices,[9] ultrafast laser writers,[10] optical switches,[11] optical parametric oscillators,[12] optical modulators,[10] and holographic devices.[13] The preparation of $LiNbO_3$ materials with nanoscale dimensions has been of particular interest due to their potential applications in ferroelectric memory devices, micro-photonic devices, optical sensors, biosensors and non-linear photocatalysis.[14–19] Nanoparticles of $LiNbO_3$ have also been used as second harmonic generation (SHG) imaging probes and have potential applications in expanding SHG based microscopy techniques.[20–22] Recently, $LiNbO_3$ nanoparticles have been used as bio-imaging probes to image cells by taking advantage of the exceptional SHG properties of these particles.[23–25] A wider utilization of nanoparticles as SHG bio-imaging probes will require their dimensions to be below 100 nm.[26,27] The NLO properties of nanomaterials can also depend on their size, shape, and/or specific chemical composition.[26] Other physical properties of perovskite based nanomaterials, such as ferroelectricity and piezoelectricity can also be strongly dependent upon their particle size

and shape.[28,29] To meet the needs of applications that seek to utilize these properties, different synthetic routes have been sought to prepare uniform nanoparticles of $LiNbO_3$.

The methods used to prepare nanomaterials of $LiNbO_3$ include solid state chemistry, molten salt syntheses, sol-gel methods, and solution-phase syntheses.[30] Molten salt syntheses and solid state methods, in particular, have been commonly used to prepare single crystals and anisotropic nanostructures of $LiNbO_3$.[31,32] Disadvantages associated with some solid state methods include a relatively high degree of aggregation in the products, a lack of the ability to tune the size of the product, a need for high temperature treatment (>500 ^oC), and the inclusion of micron sized particles.[30,33] Sol-gel methods are widely reported in the literature to prepare nanomaterials and nanocrystalline thin films of $LiNbO_3$. Limitations associated with some sol-gel processes is the need for a calcination step to induce crystallization in the products, and the formation of aggregated nanostructures.[34,35] The Pechini technique, a wet chemical method that uses polymeric precursors, has also been used to prepare nanoparticles of $LiNbO_3$. This technique does, however, have limitations that include the need for high temperature calcination (~500 ^oC) and the formation of a relatively aggregated product.[36,37] Solution-phase methods have been sought to overcome many of these limitations.

A number of solution-phase methods are reported in the literature for the preparation of $LiNbO_3$ nanomaterials. Many of these methods can provide good control over the size, shape and purity of $LiNbO_3$ nanomaterials. The solution-phase approach to prepare $LiNbO_3$ can also provide access to relatively low temperature processes, less aggregated products and an ability to incorporate a wide range of reagents.[37] Limitations associated with some of the previously demonstrated solution-phase methods include the formation of some micrometer size by-products, relatively long reaction times, and/or multi-step processing of the products.[37–42] To the best of our

knowledge, very few reports have been published in the literature demonstrating methods to prepare $LiNbO_3$ nanoparticles with diameters below 100 nm. Antonietti *et al*. reported the synthesis of $LiNbO_3$ nanoparticles with diameters between 30 to 90 nm using a solution-phase synthesis. This approach required an inert atmosphere for handling the reagents (e.g., lithium metal), 4 days to carry out the reaction, and yielded a product containing a wide range of particle sizes and non-uniform shapes.[43] In a separate study, Wiley *et al.* prepared $LiNbO_3$ nanoparticles with an average size of 50 nm through a solvothermal method using 1,4-butandiol, a controlled substance, as a solvent. This method required 3 days to carry out the reaction.[14] Our group previously reported the preparation of spherical and anisotropic $LiNbO_3$ nanoparticles via the thermal decomposition of a single source precursor through a solution-phase synthesis that also required a 1 to 2 day process. Average lengths and diameters of the anisotropic nanoparticles were 100 nm and 7 nm, respectively. This approach used an inert atmosphere for processing the reagents, temperatures above 350 ^oC to initiate decomposition of the precursor, and the product contained some non-uniform shapes.[44] An alternative synthetic approach was sought for preparing $LiNbO_3$ nanoparticles with a uniform shape and size, as well as the use of simpler and shorter processing conditions.

Here, we report a surfactant assisted solution-phase synthesis of $LiNbO_3$ nanoparticles. To the best of our knowledge, this is the first report to prepare uniform $LiNbO_3$ nanoparticles with diameters down to 30 nm through the use of a solvothermal process with a relatively short reaction time. This solution-phase approach to prepare $LiNbO_3$ nanoparticles has a number of advantages, such as processing times as short as 36 h, and reaction temperatures down to 220 ^oC without the need for further heat treatment or the use of an inert atmosphere. The $LiNbO_3$ nanoparticles prepared by this route were assessed as a function of reaction time (e.g., 24 h to 96 h) to probe the

mechanism of their formation and to assess the evolution of their dimensions and shape. These particles were also demonstrated to be optically active for SHG.

Experimental Section

Synthesis of Lithium Niobate Nanoparticles

All the chemicals were of analytical grade and were used as received without further purification. Lithium niobate nanoparticles were prepared in a single step through a solvothermal process. In brief, 40 mM of niobium ethoxide [($Nb(OC_2H_5)_5$, >90%, Gelest Inc.] was dissolved in 10.0 mL of benzyl alcohol (99%, Acros Organics) and stirred for 30 min, which resulted in the formation of a pale yellow solution. This step was followed by the addition of 0.1 mL (i.e. 72 mM) of triethylamine [$N(C_2H_5)_3$, 99%, Anachemia], which served as a surfactant to assist in controlling the growth and colloidal stability of the nanocrystals. The mixture was stirred for another 30 min. After this period of time, 40 mM of lithium hydroxide monohydrate ($LiOH \cdot H_2O$, 99%, Alfa Aesar) was added to the solution, which was stirred for another 10 h at room temperature. The resulting mixture was transferred to a 23 mL Teflon lined autoclave (Model No. 4749, Parr Instruments Co., Moline, IL USA) and heated at 220 ^oC for a specific period of time ranging from 24 to 96 h. After cooling to room temperature, white precipitates were isolated from the solution via a process of centrifugation (Model No. AccuSpin 400, Fisher Scientific) at 8000 rpm for 20 min and decanting of the solution. These solids were washed three times by re-suspending with 10 mL of ethanol and repeating the process of centrifugation and decanting of the solution. The purification process was repeated three more times with 10 mL of deionized water (18 MΩ·cm, produced using a Barnstead NANOpure DIamond water filtration system). The purified product was dried at 70 ^oC for 12 h to remove residual water prior to further analyses.

Characterization of Lithium Niobate Nanoparticles

The morphology, dimensions, crystallinity, and lattice parameters of the $LiNbO_3$ nanoparticles were characterized using an FEI Osiris X-FEG 8 transmission electron microscope (TEM) operated at an accelerating voltage of 200 kV. The TEM was calibrated using a thin film of aluminum before acquiring selected area electron diffraction (SAED) patterns from the samples. The camera length was 220 mm. Samples for TEM analysis were prepared by dispersing the purified products in ethanol followed by drop casting 5 µL of each suspension onto separate TEM grids (300 mesh copper grids coated with formvar/carbon) purchased from Cedarlane Labs. Each TEM grid was dried at ~230 Torr for at least 20 min prior to analysis. The TEM aperture used to acquire SAED patterns from multiple nanoparticles and the diffraction from a single nanoparticle were was 40 µm and 10 µm, respectively.

Phase and crystallinity of the samples were further determined from X-ray diffraction (XRD) patterns acquired with a Rigaku R-Axis Rapid diffractometer equipped with a 3 kW sealed tube copper source (Kα radiation, $\lambda = 0.15418$ nm) collimated to 0.5 mm. Powder samples were packed into a cylindrical recess drilled into a glass microscope slide (Leica 1 mm Surgipath Snowcoat X-tra Micro Slides) for acquiring XRD patterns of the products.

Purity and phase of the product with respect to the desired rhombohedral phase were further assessed using Raman spectroscopy techniques. Raman spectra were collected using a Renishaw inVia Raman microscope with a 50X LWD objective lens (Leica, 0.5 NA), and a 514 nm laser (argon ion laser, Model No. Stellar-Pro 514/50) set to 100% laser power with an exposure time of 30 s. The Raman spectrometer was calibrated by collecting the Raman spectrum of a polished silicon (Si) standard with a distinct peak centered at 520 cm^{-1}. The Raman spectra for the samples

were acquired from 100 to 1000 cm^{-1} using a 1200 lines/mm grating and a scan rate of 30 cm^{-1} per second.

The SHG activity of the $LiNbO_3$ nanoparticles were assessed using a Leica SP5 laser scanning confocal two photon microscope equipped with a Coherent Chameleon Vision II laser and a 20X objective lens (Leica, 1.0 NA). Dried powders of the $LiNbO_3$ nanoparticles were loaded onto glass cover slips and brought into the focal point of the microscope. The excitation wavelength was set to either 800 nm or 900 nm, and the corresponding band-pass filters were centered on 400 nm or 450 nm, respectively, to selectively collect the SHG signals.

Results and Discussion

We sought to develop a surfactant assisted solution-phase method to prepare single-crystalline nanoparticles of $LiNbO_3$ with uniform sizes and shapes. This surfactant assisted solution-phase approach to prepare $LiNbO_3$ nanoparticles used niobium ethoxide and lithium hydroxide monohydrate as precursors. These reagents were reacted in the presence of triethylamine, which served as a surfactant during formation of the $LiNbO_3$ nanoparticles. These reagents were dissolved in benzyl alcohol along with the triethylamine. Triethylamine, a short chain tertiary amine, was selected to passivate the surfaces of the nanocrystals during their growth and to minimize aggregation of the resulting nanoparticles.[45] Niobium (V) ions are known to form labile complexes in which weaker coordinating ligands can be replaced by stronger ligands. Benzyl alcohol can act as a coordinating solvent due to its lower pKa value (e.g., 15.40) than ethanol (e.g., 15.9), which results in a process of ligand exchange on the niobium.[46–49] The ethoxide groups ($C_2H_5O^-$) originally coordinated with the niobium (Nb^{5+}) were exchanged with benzoxide groups ($C_7H_7O^-$). This ligand exchange process resulted in a simultaneous change in the appearance of the

solution from colorless to a pale yellow. Triethylamine is also known to coordinate with the metal ions and may also interact with the niobium complexes in the solution to form adducts.[49] Hydrolysis of the niobium precursor likely occurs upon the addition of the lithium hydroxide monohydrate to this solution, resulting in the formation of niobium hydroxide. During the solvothermal treatment, these niobium hydroxide and lithium hydroxide precursors react further to form $LiNbO_3$ nanoparticles. Solvothermal treatment of the precursors was performed at 220 ^oC over a period of time from 24 to 96 h.

A proposed growth mechanism of the $LiNbO_3$ nanoparticles is shown in Figure 1. The products prepared at 24 and 30 h contained agglomerated nanoparticles with average diameters less than 10 nm. A number of larger nanoparticles with dimensions between 20 and ~50 nm were also observed in the product at 30 h (Figures 2 and S1), indicating a bimodal size distribution at this stage of the reaction. This result is distinct from what is observed during a process that is only driven by Ostwald ripening.[50,51] This increase in dimensions of the nanoparticles with progression of the reaction up to 30 h was instead attributed to a controlled agglomeration of the smaller nanoparticles, which was mediated by the presence of the triethylamine surfactant. Agglomeration of the smaller nanoparticles is attributed to their relatively high chemical potential due to their larger surface to volume ratio. These relatively small nanoparticles also have a greater mobility in solution, which increases their frequency of collision and enhances their probability to agglomerate.[52] A further increase in the reaction time to 36 h resulted in the formation of a relatively well-dispersed and uniform product of $LiNbO_3$ nanoparticles with average dimensions of 30 ± 5 nm (Figures 2 and S2). This further increase in particle size and the improvement in its uniformity were attributed to further growth of nanoparticles via processes of oriented attachment and Ostwald ripening. During Ostwald ripening, the higher chemical potential of the smaller

nanoparticles relative to the larger nanoparticles leads to a faster dissolution of the smaller particles in the solution.[52] The larger nanoparticles are more stable due to their smaller chemical potential and they tend to progressively grow into larger nanoparticles. The potential dissolution of the smaller nanoparticles could generate monomeric or similar species in the solution, and the larger nanoparticles subsequently grow from addition of these highly reactive species to their surfaces.[50,51,53] Under normal conditions, a process dominated by Ostwald ripening produces a unimodal size distribution, which is distinct from the size distribution observed in the early stages of this reaction. The size distribution of nanoparticles grown by Ostwald ripening can also broaden and shift to larger dimensions during subsequent coarsening processes (Figure 2).

The growth of nanoparticles during the later stages of the reaction proceeds through deposition of material onto either individual nanoparticles or onto agglomerates of these nanoparticles. The mechanism of growth can be distinguished by analyzing the structure of the resulting nanoparticles. The nanoparticles grown through an oriented attachment process followed by Ostwald ripening usually consist of a single crystal domain, but Ostwald ripening of agglomerates (or aggregates) can result in polycrystalline particles and potentially exhibit twinned crystal planes.[50] The nanoparticles obtained at a reaction time of 36 h were single-crystalline *vide infra*, which further supported the hypothesis that the nanoparticles age through a process that includes oriented attachment and Ostwald ripening. In this synthesis, a product of single-crystalline nanoparticles grew at the expense of smaller nanoparticles whether from individual or agglomerated species. As the growth proceeded at the elevated reaction temperatures, these smaller nanoparticles dissolved and contributed to the further growth of the larger nanoparticles into single-crystalline products. The driving force for this dissolution of the smaller particles, including those in the agglomerates, was from their higher chemical potential relative to the larger

single-crystalline materials. The size of the single-crystalline nanoparticles increased as the reaction progressed from 36 to 96 h. Average dimensions of the $LiNbO_3$ nanoparticles prepared at 48 h and 96 h were 55 ± 14 nm and 95 ± 20 nm, respectively (Figures 2 and S2). It is worth noting that the size distribution of the nanoparticles continues to broaden. In summary, the results suggest that the formation of the $LiNbO_3$ nanoparticles is initiated by a process of nucleation. As the reaction progressed, these relatively small nanocrystals start to agglomerate, which are reversible as their surfaces remain passivated with the triethylamine surfactant. Growth of individual nanoparticles proceeds in a controlled manner through a process of oriented attachment and Ostwald ripening to yield single-crystalline products. This secondary step of growth following the initial agglomeration of the nuclei transforms the product from a bimodal size distribution into a fairly uniform product at 36 h.

Evolution of the phase and crystallinity of the nanoparticles obtained at specific time points throughout the reaction were characterized using powder XRD analyses. The XRD patterns of the products obtained between 30 and 96 h indicated the formation of a crystalline product. All peaks were indexed with JCPDS No. 020-0631 corresponding to the formation of rhombohedral $LiNbO_3$ (Figure 3). Diffraction peaks between 2-theta values of 50° to 60° were absent for the materials prepared at a reaction time of 24 h, which indicated an incomplete crystallization of the product. In addition, the relatively broad peaks observed in the XRD patterns of the product prepared with a reaction time of 24 h indicated the presence of relatively small crystalline domains in the product (Table S1). The average dimensions of the crystallites in the products were calculated using the Scherrer equation.[54] High resolution TEM techniques were attempted to visualize the crystalline domains within the sample at 24 h, but these results were inconclusive likely due to a high degree of disorder within these samples. Analysis by SAED of the observed agglomerates did, however,

further verify that the product at 24 h was polycrystalline (Figure S3). Dimensions of the crystallites in the products prepared between 30 to 96 h were calculated for the [012], [104], [110], and [116] directions (Table S2). The peak area of the (012) reflection increased relative to the other reflections for the products prepared with longer reaction times indicating the growth of the nanoparticles along this direction during the solvothermal treatment. The relative intensities of the (110), (024), and (116) reflections decreased in the products prepared after the 36 h time point in the reaction, which indicated a non-uniform growth of the nanoparticles along the different crystalline planes. Longer reaction times resulted in a decrease in the uniformity of the product as a result of this differential growth of the crystalline facets. The average dimensions of the crystallites increased from ~21 to ~26 nm along the [012] direction with prolonged heating of the solvothermal product at 220 ^{o}C (Table S2). In contrast, the average crystalline dimensions along the other directions exhibited relatively little change throughout the duration of the reaction. The average dimensions of the nanoparticles as determined from TEM analyses of the products prepared after 48 and 96 h were significantly larger than the calculated dimensions of the crystallites. This inconsistency in the average particle size estimated from the XRD data with the measurements obtained from the TEM data is likely due to the presence of non-spherical crystallites in the products.[55] High resolution TEM analyses of the products collected at 36 to 96 h exhibit regular lattice fringe patterns (Figure S4). The observed lattice spacing matched the major reflections observed in the diffraction analyses of these products. These analyses suggested that growth by this solution-phase process was controlled by the addition of the triethylamine surfactant, which produced single-crystalline nanoparticles of $LiNbO_3$.

The evolution of the phase and crystallinity of the $LiNbO_3$ nanoparticles were evaluated further by Raman spectroscopy techniques (Figure 4). Characteristic peaks for $LiNbO_3$ were

observed in the Raman spectra for samples prepared at reaction times from 30 to 96 h, which were indexed to the formation of rhombohedral $LiNbO_3$ (Table S3).[3,14,56] The Raman spectrum of the product prepared at a reaction time of 24 h indicated that the sample did not contain $LiNbO_3$ with sufficiently large domain sizes for the detection limits of our Raman instrument, and/or that there is a relatively high degree of disorder within the sample at this early stage of the reaction. Raman spectroscopy was also utilized to confirm the purity of the $LiNbO_3$ nanocrystals. This technique can differentiate the phase, as well as the composition of the lithium niobate (e.g., $LiNbO_3$, Li_3NbO_4 and $LiNb_3O_8$).[57] A commercial $LiNbO_3$ powder was also analyzed as a reference material for comparison to the as-synthesized $LiNbO_3$ nanoparticles. The products of this solvothermal method were not treated by high temperature processes (e.g., calcination), but were directly analyzed after the purification step as outlined in the Experimental Section. The Raman spectra for the $LiNbO_3$ nanoparticles matched the spectrum for the commercial $LiNbO_3$ powder, which further indicated the formation of a pure phase of rhombohedral $LiNbO_3$ (Figures 4 and S6). Raman spectroscopy of $LiNbO_3$ is also sensitive to the nominal size of the nanoparticles (Figure 5). Significant changes can be observed in the Raman spectra of a material when comparing its bulk properties to those as a nanoparticle.[58,59] A key contribution to this observation is that nanoparticles have a higher ratio of surface atoms to bulk atoms.[58,60] Bond lengths can be different for species on the surfaces of the $LiNbO_3$, due to their lower coordination number, than those in the bulk. For example, some surface bonds can undergo a contraction due to the formation of Nb=O species. A decrease in the average size of the nanoparticles was associated with the observation of new vibrational modes in the Raman spectra. The appearance of a Raman band at ~900 cm^{-1} has been attributed to distortions of Nb=O species on the surfaces of the nanocrystals.[56,59] The relative intensity of this Raman band decreased with an increase in the average diameter of the

nanoparticles. The E-LO mode at ~870 cm^{-1} was largely unaffected by the changes in the dimensions of the nanoparticles. The TEM, XRD, and Raman results collectively confirmed that the optimal reaction time was 36 h for the formation of crystalline, uniform, and relatively small $LiNbO_3$ nanoparticles. A more detailed analysis was, therefore, performed on the product prepared at a reaction time of 36 h.

Transmission electron microscopy analyses indicated the $LiNbO_3$ nanoparticles obtained at 36 h were relatively uniform in size and that their shapes were semi-spherical (Figure 6). The average dimensions of these nanoparticles were calculated from measurements obtained from at least 250 nanoparticles. Their size distribution was unimodal with an average particle size of 30 ± 5 nm as stated above. Crystallinity and phase of these $LiNbO_3$ nanoparticles were further investigated using electron diffraction techniques. A well-defined ring pattern was observed in the SAED obtained from multiple nanoparticles, which confirmed the formation of crystalline materials (Figure 6c). The SAED pattern was indexed to $LiNbO_3$ and matched the assignment of the product to the rhombohedral phase of $LiNbO_3$. The atomic-scale crystallinity of the $LiNbO_3$ nanoparticles was analyzed by high resolution TEM or HRTEM (Figure 6d). A uniform lattice structure was observed throughout each of the nanocrystals, which suggested that each nanoparticle was a single crystal. The periodic fringe patterns observed by HRTEM for some of these nanocrystals had a spacing of 3.7 Å. This spacing matched the inter-planar spacing for the (012) planes of $LiNbO_3$ (e.g., Figure 6e). Further analysis of the HRTEM images by a Fast Fourier Transformation (FFT) (e.g., Figure 6e inset) indicated the presence of facets with {012} and {104} orientations when viewed along the $[\bar{4}\bar{2}1]$ zone axis. Electron diffraction patterns obtained from individual $LiNbO_3$ nanoparticles further indicated the single crystal nature of the product prepared after a reaction time of 36 h (Figure S7). For example, the spot pattern from one nanocrystal was

indexed to diffraction along the $[1\bar{1}0]$ zone axis of $LiNbO_3$ (Figure S7). These analyses collectively indicated the presence of {012}, {104}, {116} and {110} as major facets within the individual single-crystalline nanoparticles of $LiNbO_3$.

Purity, crystallinity, and phase of the $LiNbO_3$ nanocrystals prepared at 36 h by the solvothermal process were further analyzed using XRD techniques. The XRD patterns for a commercial $LiNbO_3$ powder (99.9%, Sigma Aldrich) were compared with these $LiNbO_3$ nanocrystals (Figure S8). The XRD patterns of the product matched well to the patterns observed for the commercial sample and to the rhombohedral structure of $LiNbO_3$ (space group R3c, JCPDS No. 020-0631).[61] Peak areas for the different XRD reflections relative to the (012) peak were determined to evaluate the presence of dominant facets in the product (Table S4). It is worth noting that the ratio of the areas of the (104)/(012), (110)/(012), and (116)/(012) peaks exhibited relatively high values of 0.65, 0.49, and 0.66, respectively, which indicates an enrichment of the {104}, {110}, and {116} facets in the $LiNbO_3$ nanocrystals relative to what is observed in larger crystals of $LiNbO_3$. The uniform dimensions of the crystallites, as determined from the Scherrer analysis of the XRD peaks, and the relatively uniform size of the nanoparticles, as determined from the TEM analysis, suggests no preferred growth direction at this stage of the reaction. Nanoparticles of $LiNbO_3$ have been previously observed to grow through a process dominated by oriented attachment.[44] The uniform growth of $LiNbO_3$ nanocrystals prepared by the solution-phase route described herein suggests there is an effective passivation of the crystal facets with inclusion of triethylamine in the reaction mixture.

Lithium niobate based materials have been widely studied for their SHG properties. The SHG response of a material is a second order nonlinear optical phenomenon in which two photons at a fundamental frequency (ω) are converted to one photon at a frequency of 2ω.[21] The SHG

properties of materials have been utilized for a number of applications that include non-linear optical microscopy, photodynamic therapy, generation of visible coherent light, and the verification of crystal structures.[21,62–64] The SHG response of the as-prepared $LiNbO_3$ nanoparticles was characterized using a two photon microscope. The $LiNbO_3$ nanocrystals exhibited a tunable SHG response. For example, the scattered wavelengths were tuned to 400 nm and 450 nm when exposed an incident laser centered at 800 nm and 900 nm, respectively (Figure S9). This SHG response of $LiNbO_3$ could be further tuned to extend across the near infrared and visible regions of the electromagnetic spectrum.[65,66] These SHG active $LiNbO_3$ nanocrystals could be used as contrast agents or markers for bio-imaging applications, as well as for enabling advanced NLO microscopy studies of the interactions between nanoparticles and live cells (e.g., cell adhesion, cell release, and enzymatic activities of cells).[19,67]

Conclusions

In summary, we demonstrated a surfactant assisted solution-phase method to prepare uniform, single-crystalline $LiNbO_3$ nanoparticles having an average size down to 30 nm. The solution-phase process to prepare these nanoparticles was carried out at a relatively low temperature (e.g., 220 ^oC) in benzyl alcohol over short reaction times (e.g., 36 h). During this solvothermal process, the precursors reacted to produce nuclei, which subsequently formed nanoparticles of $LiNbO_3$. The growth of these nanoparticles initially proceeded through a surfactant controlled agglomeration of nanoparticles. Processes of Ostwald ripening and oriented attachment dominated the later stages of this reaction, which controlled further growth of the nanoparticles. The resulting nanoparticles of $LiNbO_3$ exhibited minimal aggregation. The optimal reaction time to prepare small and uniform nanocrystals of $LiNbO_3$ was 36 h. Their size could be

further tuned by increasing the reaction time. Phase and purity of the products were characterized by XRD and Raman spectroscopy and compared to a commercially available $LiNbO_3$ powder. These results indicated the formation of a pure rhombohedral phase of $LiNbO_3$ at a relatively low temperature (e.g., 220 ^oC). The 30-nm diameter $LiNbO_3$ nanocrystals contain {110}, {104}, {116}, and {012} as major facets as characterized through SAED, HRTEM and XRD analyses. The results of these analyses suggested that there was no preferred growth direction at this stage of the reaction, which resulted in the formation of semi-spherical nanoparticles of $LiNbO_3$. The product was also SHG active and could be explored in the future for use as SHG imaging probes for applications requiring long-term monitoring of biological or other systems.

Acknowledgements

This work was supported in part by the Natural Sciences and Engineering Research Council (NSERC) of Canada (Discovery Grant No. 1077758), and through the Collaborative Health Research Projects (CHRP) Partnership Program supported in part by the Canadian Institutes of Health Research (Grant No. 134742) and the NSERC of Canada (Grant No. 462260), the Canada Research Chairs Program (B.D. Gates, Grant No. 950-215846) and CMC Microsystems (MNT Financial Assistance Grant No. 4279). This work made use of 4D LABS (www.4dlabs.com) and the Center for Soft Materials shared facilities supported by the Canada Foundation for Innovation (CFI), British Columbia Knowledge Development Fund (BCKDF), Western Economic Diversification Canada, and Simon Fraser University. The authors also thank Dr. Saeid Kamal (4D LABS) for discussions and helping to acquire SHG spectra of the samples.

Supporting Information

The supporting information is available free of charge on the ACS Publications website. This file includes additional crystallographic results, transmission and scanning electron microscopy data, Raman spectra, particle size analyses, and second harmonic generation spectra for the nanocrystals of $LiNbO_3$.

References

(1) Schröder, M.; Haußmann, A.; Thiessen, A.; Soergel, E.; Woike, T.; Eng, L. M. Conducting Domain Walls in Lithium Niobate Single Crystals. *Adv. Funct. Mater.* **2012**, *22*, 3936–3944.

(2) Xue, D.; Kitamura, K. Crystal Structure and Ferroelectricity of Lithium Niobate Crystals. *Ferroelectrics* **2003**, *297*, 19–27.

(3) Chen, Z.; Huang, J.; Yang, Y.; Wang, Y.; Wu, Y.; He, H.; Wei, X.; Ye, Z.; Zeng, H.; Cong, H. Piezoelectric Properties of Rhombic $LiNbO_3$ Nanowires. *RSC Adv.* **2012**, *2*, 7380–7383.

(4) Grange, R.; Choi, J.-W.; Hsieh, C.-L.; Pu, Y.; Magrez, A.; Smajda, R.; Forró, L.; Psaltis, D. Lithium Niobate Nanowires Synthesis, Optical Properties, and Manipulation. *Appl. Phys. Lett.* **2009**, *95*, 143105.

(5) Bhatt, R.; Bhaumik, I.; Ganesamoorthy, S.; Bright, R.; Soharab, M.; Karnal, A. K.; Gupta, P. K. Control of Intrinsic Defects in Lithium Niobate Single Crystal for Optoelectronic Applications. *Crystals* **2017**, *7*, 23, 1-20.

(6) Kösters, M.; Sturman, B.; Werheit, P.; Haertle, D.; Buse, K. Optical Cleaning of Congruent Lithium Niobate Crystals. *Nat. Photonics* **2009**, *3*, 510–513.

(7) Nikogosyan, D. N. *Nonlinear Optical Crystals: A Complete Survey*; Springer Science & Business Media, 2006; *pp* 5–54.

(8) Wang, C.; Burek, M. J.; Lin, Z.; Atikian, H. A.; Venkataraman, V.; Huang, I.-C.; Stark, P.; Lončar, M. Integrated High Quality Factor Lithium Niobate Microdisk Resonators. *Opt. Express* **2014**, *22*, 30924–30933.

(9) Pidgeon, C. R.; Colles, M. J. Recent Developments in Tunable Lasers for Spectroscopy. *Nature* **1979**, *279*, 377–381.

(10) Guarino, A.; Poberaj, G.; Rezzonico, D.; Degl'Innocenti, R.; Günter, P. Electro–optically Tunable Microring Resonators in Lithium Niobate. *Nat. Photonics* **2007**, *1*, 407–410.

(11) Shang, J.; Sun, J.; Li, Q.; Yang, J.; Zhang, L.; Xu, J. Single-Block Pulse-on Electro-Optic Q-Switch Made of $LiNbO_3$. *Sci. Rep.* **2017**, *7*, 1-7.

(12) Dunn, M. H.; Ebrahimzadeh, M. Parametric Generation of Tunable Light from Continuous-Wave to Femtosecond Pulses. *Science.* **1999**, *286*, 1513–1517.

(13) Buse, K.; Adibi, A.; Psaltis, D. Non-Volatile Holographic Storage in Doubly Doped Lithium Niobate Crystals. *Nature* **1998**, *393*, 665–668.

(14) Mohanty, D.; Chaubey, G. S.; Yourdkhani, A.; Adireddy, S.; Caruntu, G.; Wiley, J. B. Synthesis and Piezoelectric Response of Cubic and Spherical $LiNbO_3$ Nanocrystals. *RSC Adv.* **2012**, *2*, 1913–1916.

(15) Saito, K.; Koga, K.; Kudo, A. Lithium Niobate Nanowires for Photocatalytic Water Splitting. *Dalt. Trans.* **2011**, *40*, 3909–3913.

(16) Liu, G.; You, S.; Ma, M.; Huang, H.; Ren, N. Removal of Nitrate by Photocatalytic Denitrification Using Nonlinear Optical Material. *Environ. Sci. Technol.* **2016**, *50*, 11218–11225.

(17) Marchesano, V.; Gennari, O.; Mecozzi, L.; Grilli, S.; Ferraro, P. Effects of Lithium Niobate Polarization on Cell Adhesion and Morphology. *ACS Appl. Mater. Interfaces* **2015**, *7*, 18113–18119.

(18) Peng, L.-H.; Wu, H.-M.; Kung, A. H.; Lai, C.-M. Fabrication and Characterization of Self-Assembled Ferroelectric Linear and Nonlinear Photonic Crystals: GaN and $LiNbO_3$. In *Ferroelectric Crystals for Photonic Applications*; Springer, 2009; pp 21–51.

(19) Toss, H.; Lönnqvist, S.; Nilsson, D.; Sawatdee, A.; Nissa, J.; Fabiano, S.; Berggren, M.;

Kratz, G.; Simon, D. T. Ferroelectric Surfaces for Cell Release. *Synth. Met.* **2017**, *228*, 99–104.
(20) Sergeyev, A.; Geiss, R.; Solntsev, A. S.; Steinbrück, A.; Schrempel, F.; Kley, E.-B.; Pertsch, T.; Grange, R. Second-Harmonic Generation in Lithium Niobate Nanowires for Local Fluorescence Excitation. *Opt. Express* **2013**, *21*, 19012–19021.
(21) Bonacina, L. Nonlinear Nanomedecine: Harmonic Nanoparticles toward Targeted Diagnosis and Therapy. *Mol. Pharm.* **2012**, *10*, 783–792.
(22) Wood, B. D. A Nonhydrolytic Solution-Phase Synthesis of Lithium Niobate Nanostructures. M.Sc. Dissertation, Simon Fraser University, Canada, **2009**.
(23) Wang, Y.; Zhou, X. Y.; Chen, Z.; Cai, B.; Ye, Z. Z.; Gao, C. Y.; Huang, J. Y. Synthesis of Cubic $LiNbO_3$ Nanoparticles and Their Application in Vitro Bioimaging. *Appl. Phys. A* **2014**, *117*, 2121–2126.
(24) Kotopoulis, S.; Wang, H.; Cochran, S.; Postema, M. Lithium Niobate Transducers for MRI-Guided Ultrasonic Microsurgery. *IEEE Trans. Ultrason. Ferroelectr. Freq. Control* **2011**, *58*, 1570–1576.
(25) Li, J.; Qiu, J.; Guo, W.; Wang, S.; Ma, B.; Mou, X.; Tanes, M.; Jiang, H.; Liu, H. Cellular Internalization of $LiNbO_3$ Nanocrystals for Second Harmonic Imaging and the Effects on Stem Cell Differentiation. *Nanoscale* **2016**, *8*, 7416–7422.
(26) Tong, L.; Cheng, J.-X. Label-Free Imaging through Nonlinear Optical Signals. *Mater. Today* **2011**, *14*, 264–273.
(27) Nune, S. K.; Gunda, P.; Thallapally, P. K.; Lin, Y.-Y.; Laird Forrest, M.; Berkland, C. J. Nanoparticles for Biomedical Imaging. *Expert Opin. Drug Deliv.* **2009**, *6*, 1175–1194.
(28) Mao, Y.; Zhou, H.; Wong, S. S. Synthesis, Properties, and Applications of Perovskite-Phase Metal Oxide Nanostructures. *Mater. Matters* **2010**, *5*, 50–58.
(29) Zhang, Y.; Liu, J.; Wang, Z.; Xue, Y.; Ou, Q.; Polavarapu, L.; Zheng, J.; Qi, X.; Bao, Q. Synthesis, Properties, and Optical Applications of Low-Dimensional Perovskites. *Chem. Commun.* **2016**, *52*, 13637–13655.
(30) Grange, R.; Dutto, F.; Radenovic, A. Niobates Nanowires: Synthesis, Characterization and Applications. In *Nanowires-Implementations and Applications*; InTech, 2011; pp 509–524.
(31) Shigematsu, K.; Anzai, Y.; Morita, S.; Yamada, M.; Yokoyama, H. Growth Conditions of Subgrain-Free $LiNbO_3$ Single Crystals by the Czochralski Method. *Jpn. J. Appl. Phys.* **1987**, *26*, 1988-1996.
(32) Santulli, A. C.; Zhou, H.; Berweger, S.; Raschke, M. B.; Sutter, E.; Wong, S. S. Synthesis of Single-Crystalline One-Dimensional $LiNbO_3$ Nanowires. *CrystEngComm* **2010**, *12*, 2675–2678.
(33) Li, L.; Deng, J.; Chen, J.; Xing, X. Topochemical Molten Salt Synthesis for Functional Perovskite Compounds. *Chem. Sci.* **2016**, *7*, 855–865.
(34) Zeng, H. C.; Tung, S. K. Synthesis of Lithium Niobate Gels Using a Metal Alkoxide− Metal Nitrate Precursor. *Chem. Mater.* **1996**, *8*, 2667–2672.
(35) Wang, L. H.; Yuan, D. R.; Duan, X. L.; Wang, X. Q.; Yu, F. P. Synthesis and Characterization of Fine Lithium Niobate Powders by Sol-gel Method. *Cryst. Res. Technol.* **2007**, *42*, 321–324.
(36) Yerlikaya, C.; Ullah, N.; Kamali, A. R.; Kumar, R. V. Size-Controllable Synthesis of Lithium Niobate Nanocrystals Using Modified Pechini Polymeric Precursor Method. *J. Therm. Anal. Calorim.* **2016**, *125*, 17–22.
(37) Graça, M. P. F.; Prezas, P. R.; Costa, M. M.; Valente, M. A. Structural and Dielectric

Characterization of $LiNbO_3$ Nano-Size Powders Obtained by Pechini Method. *J. Sol-Gel Sci. Technol.* **2012**, *64*, 78–85.
(38) Liu, M.; Xue, D. Amine-Assisted Route to Fabricate $LiNbO_3$ Particles with a Tunable Shape. *J. Phys. Chem. C* **2008**, *112*, 6346–6351.
(39) Nyman, M.; Anderson, T. M.; Provencio, P. P. Comparison of Aqueous and Non-Aqueous Soft-Chemical Syntheses of Lithium Niobate and Lithium Tantalate Powders. *Cryst. Growth Des.* **2008**, *9*, 1036–1040.
(40) Camargo, E. R.; Kakihana, M. Chemical Synthesis of Lithium Niobate Powders ($LiNbO_3$) Prepared from Water-Soluble DL-Malic Acid Complexes. *Chem. Mater.* **2001**, *13*, 1905–1909.
(41) Zhao, L.; Steinhart, M.; Yosef, M.; Lee, S. K.; Geppert, T.; Pippel, E.; Scholz, R.; Gösele, U.; Schlecht, S. Lithium Niobate Microtubes within Ordered Macroporous Silicon by Templated Thermolysis of a Single Source Precursor. *Chem. Mater.* **2005**, *17*, 3–5.
(42) Wohlrab, S.; Weiss, M.; Du, H.; Kaskel, S. Synthesis of $MNbO_3$ Nanoparticles (M= Li, Na, K). *Chem. Mater.* **2006**, *18*, 4227–4230.
(43) Niederberger, M.; Pinna, N.; Polleux, J.; Antonietti, M. A General Soft-chemistry Route to Perovskites and Related Materials: Synthesis of $BaTiO_3$, $BaZrO_3$, and $LiNbO_3$ Nanoparticles. *Angew. Chemie.* **2004**, *116*, 2320–2323.
(44) Wood, B. D.; Mocanu, V.; Gates, B. D. Solution-Phase Synthesis of Crystalline Lithium Niobate Nanostructures. *Adv. Mater.* **2008**, *20*, 4552–4556.
(45) Bakshi, M. S. How Surfactants Control Crystal Growth of Nanomaterials. *Cryst. Growth Des.* **2015**, *16*, 1104–1133.
(46) Bradley, D. C.; Charkravarti, B. N.; Chatterjee, A. K.; Wardlaw, W.; Whitley, A. 19. Niobium and Tantalum Mixed Alkoxides. *J. Chem. Soc.* **1958**, 99–101.
(47) Dengel, A. C.; Griffith, W. P. Studies on Transition Metal Peroxo complexes—IX. Carboxylato Peroxo Complexes of Niobium(V), Tantalum(V), Zirconium(IV) and Hafnium(IV). *Polyhedron* **1989**, *8*, 1371–1377.
(48) Niederberger, M.; Garnweitner, G. Organic Reaction Pathways in the Nonaqueous Synthesis of Metal Oxide Nanoparticles. *Chem. Eur. J.* **2006**, *12*, 7282–7302.
(49) Qamar, M.; Abdalwadoud, M.; Ahmed, M. I.; Azad, A.-M.; Merzougui, B.; Bukola, S.; Yamani, Z. H.; Siddiqui, M. N. Single-Pot Synthesis Of ⟨001⟩-Faceted N-Doped Nb_2O_5/Reduced Graphene Oxide Nanocomposite for Efficient Photoelectrochemical Water Splitting. *ACS Appl. Mater. Interfaces* **2015**, *7*, 17954–17962.
(50) Wang, F.; Richards, V. N.; Shields, S. P.; Buhro, W. E. Kinetics and Mechanisms of Aggregative Nanocrystal Growth. *Chem. Mater.* **2013**, *26*, 5–21.
(51) Polte, J. Fundamental Growth Principles of Colloidal Metal Nanoparticles–A New Perspective. *CrystEngComm* **2015**, *17*, 6809–6830.
(52) Zheng, H.; Smith, R. K.; Jun, Y.; Kisielowski, C.; Dahmen, U.; Alivisatos, A. P. Observation of Single Colloidal Platinum Nanocrystal Growth Trajectories. *Science.* **2009**, *324*, 1309–1312.
(53) Thanh, N. T. K.; Maclean, N.; Mahiddine, S. Mechanisms of Nucleation and Growth of Nanoparticles in Solution. *Chem. Rev.* **2014**, *114*, 7610–7630.
(54) Patterson, A. L. The Scherrer Formula for X-Ray Particle Size Determination. *Phys. Rev.* **1939**, *56*, 978–982.
(55) Wang, Y.; Chan, S. L. I.; Amal, R.; Shen, Y. R.; Kiatkittipong, K. XRD Anisotropic Broadening of Nano-crystallites. *Powder Diffr.* **2010**, *25*, 217-217.

(56) Jehng, J. M.; Wachs, I. E. Structural Chemistry and Raman Spectra of Niobium Oxides. *Chem. Mater.* **1991**, *3*, 100–107.
(57) Bartasyte, A.; Plausinaitiene, V.; Abrutis, A.; Stanionyte, S.; Margueron, S.; Boulet, P.; Kobata, T.; Uesu, Y.; Gleize, J. Identification of $LiNbO_3$, $LiNb_3O_8$ and Li_3NbO_4 Phases in Thin Films Synthesized with Different Deposition Techniques by Means of XRD and Raman Spectroscopy. *J. Phys. Condens. Matter* **2013**, *25*, 205901.
(58) Gao, Y.; Zhao, X.; Yin, P.; Gao, F. Size-Dependent Raman Shifts for Nanocrystals. *Sci. Rep.* **2016**, *6*, 1-5.
(59) Kreissl, H. T.; Li, M. M.-J.; Peng, Y.-K.; Nakagawa, K.; Hooper, T.; Hanna, J. V; Shepherd, A. M.; Wu, T.-S.; Soo, Y.-L.; Tsang, S. C. E. Structural Studies of Bulk to Nano-Size Niobium Oxides with Correlation to Their Acidity. *J. Am. Chem. Soc.* **2017**, *139*, 12670–12680.
(60) Yang, C. C.; Li, S. Size-Dependent Raman Red Shifts of Semiconductor Nanocrystals. *J. Phys. Chem. B* **2008**, *112*, 14193–14197.
(61) Luo, C.; Xue, D. Mild, Quasireverse Emulsion Route to Submicrometer Lithium Niobate Hollow Spheres. *Langmuir* **2006**, *22*, 9914–9918.
(62) Rogov, A.; Mugnier, Y.; Bonacina, L. Harmonic Nanoparticles: Noncentrosymmetric Metal Oxides for Nonlinear Optics. *J. Opt.* **2015**, *17*, 33001.
(63) Tran, T. T.; Yu, H.; Rondinelli, J. M.; Poeppelmeier, K. R.; Halasyamani, P. S. Deep Ultraviolet Nonlinear Optical Materials. *Chem. Mater* **2016**, *28*, 5238–5258.
(64) Schmitt, P. D. Recent Advances in Nonlinear Optical Analyses of Pharmaceutical Materials in the Solid State. *Mol. Pharm.* **2017**, *14*, 555–565.
(65) Shadrivov, I. V; Lapine, M.; Kivshar, Y. S. *Nonlinear, Tunable and Active Metamaterials*; Springer, 2015; pp 1–129.
(66) Cai, F.; Yu, J.; Qian, J.; Wang, Y.; Chen, Z.; Huang, J.; Ye, Z.; He, S. Use of Tunable Second-harmonic Signal from $KNbO_3$ Nanoneedles to Find Optimal Wavelength for Deep-tissue Imaging. *Laser Photon. Rev.* **2014**, *8*, 865–874.
(67) Vaněk, P.; Kolská, Z.; Luxbacher, T.; García, J. A. L.; Lehocký, M.; Vandrovcová, M.; Bačáková, L.; Petzelt, J. Electrical Activity of Ferroelectric Biomaterials and Its Effects on the Adhesion, Growth and Enzymatic Activity of Human Osteoblast-like Cells. *J. Phys. D. Appl. Phys.* **2016**, *49*, 175403.

Figures and Captions

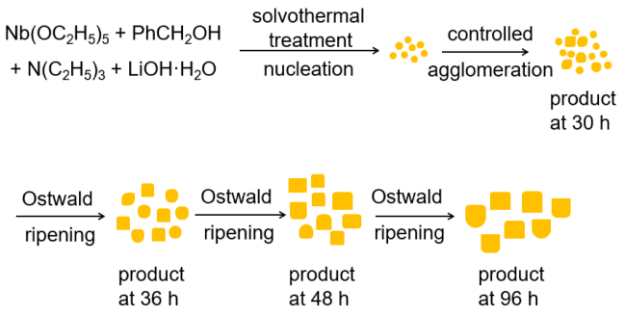

Figure 1. A proposed mechanism for the synthesis of $LiNbO_3$ nanocrystals through a solution-phase process. The solvothermal treatment of the precursors produced nuclei that formed nanoparticles of $LiNbO_3$. The growth of these nanoparticles initially followed a process of controlled agglomeration, but a process of Ostwald ripening dominated their subsequent growth with further heating of the reaction mixture.

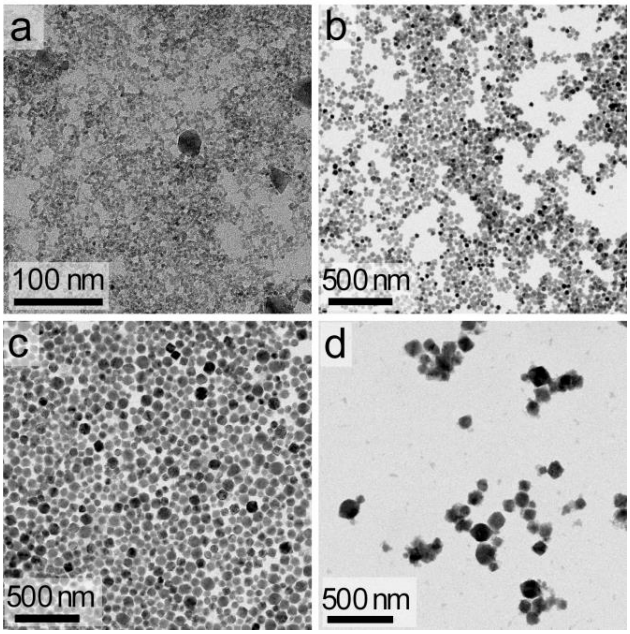

Figure 2. Transmission electron microscopy (TEM) analyses of $LiNbO_3$ nanoparticles obtained after a reaction time of: (a) 30 h; (b) 36 h; (c) 48 h; and (d) 96 h.

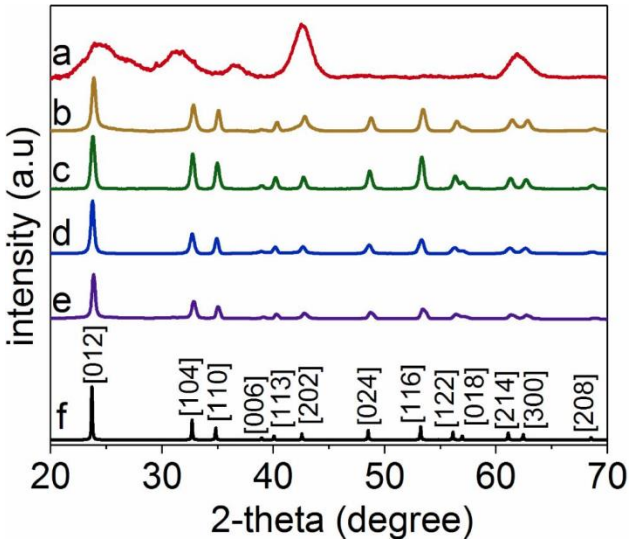

Figure 3. Powder X-ray diffraction (XRD) patterns of $LiNbO_3$ nanoparticles obtained after a reaction time of: (a) 24 h; (b) 30 h; (c) 36 h; (d) 48 h; and (e) 96 h. Also included are XRD patterns for (f) a reported $LiNbO_3$ reference (JCPDS No. 020-0631).

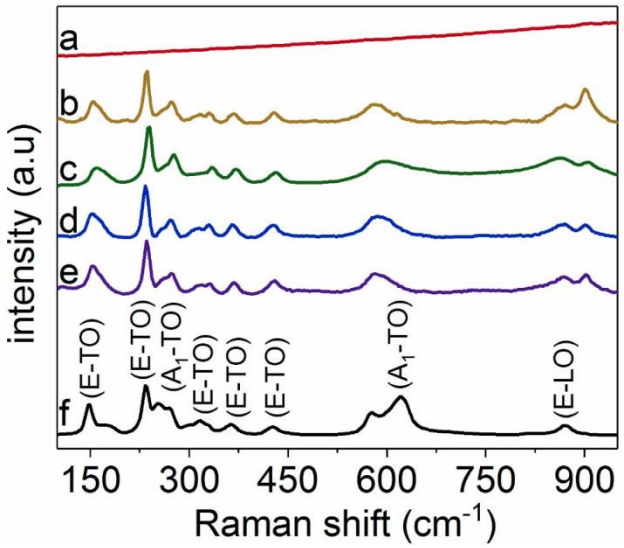

Figure 4. Analyses by Raman spectroscopy of $LiNbO_3$ nanoparticles obtained after a reaction time of: (a) 24 h; (b) 30 h; (c) 36 h; (d) 48 h; and (e) 96 h. Data is also included for (f) a commercial $LiNbO_3$ powder.

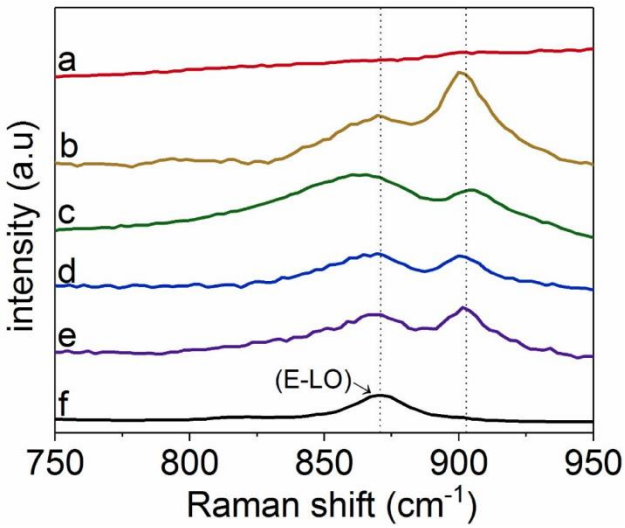

Figure 5. Raman spectra depicting the E-LO bands of $LiNbO_3$ nanoparticles obtained after a reaction time of: (a) 24 h; (b) 30 h; (c) 36 h; (d) 48 h; and (e) 96 h. Data is also included for (f) a commercial powder of micrometer size $LiNbO_3$ particles. Vertical lines overlapping the spectra indicate the vibrations observed at ~870 cm^{-1} and ~900 cm^{-1}.

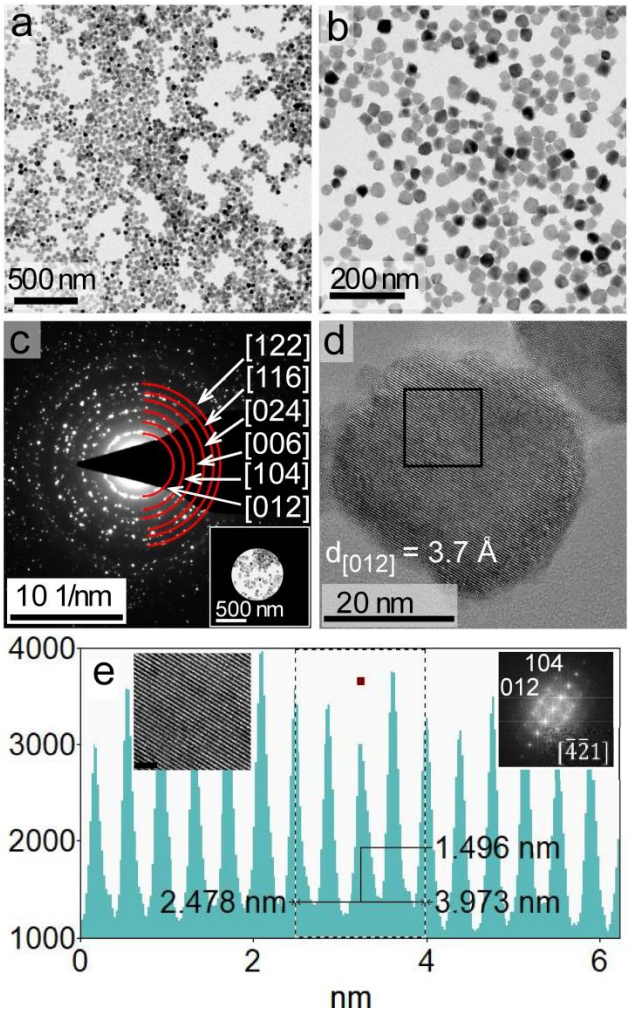

Figure 6. Lithium niobate nanoparticles obtained after a 36 h solvothermal process as characterized by: (a, b) TEM; (c) selected area electron diffraction (SAED); and (d) high resolution (HR) TEM. (e) Detailed analyses of the d-spacing and crystallographic orientation of the nanocrystal observed in (d). Insets depict a magnified view of the HRTEM image (scale bar = 2 nm) corresponding to the box in (d) obtained along the $[\bar{4}\bar{2}1]$ zone axis, and an analysis of this HRTEM image by a Fast Fourier Transformation (FFT). These analyses further confirmed the single-crystallinity of the nanoparticle.

TOC Graphic

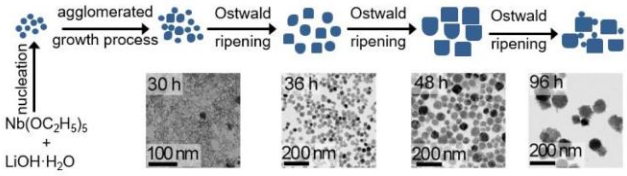
agglomerated
growth process
Ostwald
ripening
Ostwald
ripening
Ostwald
ripening
nucleation
Nb(OC2H5)5
+
LiOH·H2O
30 h
100 nm
36 h
200 nm
48 h
200 nm
96 h
200 nm